Two-dimensional and π plasmon spectra in pristine and doped graphene

V. Despoja,[1,2,3,*] D. Novko,[1] K. Dekanić,[1] M. Šunjić,[1,2] and L. Marušić[4]

[1]*Department of Physics, University of Zagreb, Bijenička 32, HR-10000 Zagreb, Croatia*

[2]*Donostia International Physics Center (DIPC), P. Manuel de Lardizabal, 20018 San Sebastian, Basque Country, Spain*

[3]*Universidad del Pais Vasco, Centro de Fisica de Materiales CSIC-UPV/EHU-MPC, Avenida Tolosa 72, E-20018 San Sebastian, Spain*

[4]*Maritime Department, University of Zadar, M. Pavlinovića b.b., HR-23000 Zadar, Croatia*

(Received 7 September 2012; revised manuscript received 4 December 2012; published 27 February 2013)

The spectra of electronic excitations in graphene are calculated using first principles time-dependent density functional theory formalism, and used to obtain π and $\pi+\sigma$ plasmon dispersion curves. The spectra and dispersion are in excellent agreement with recent experimental results, and they are used to investigate the anisotropy and splitting of a π plasmon, which has also been experimentally verified. The high accuracy of this calculation enabled the discovery of some different features in the spectra, especially the ΓM-ΓK anisotropy of the two-dimensional (2D) plasmon dispersion curve, which qualitatively agrees with recent experimental results. Our *ab initio* 2D plasmon dispersion curves are compared with the ones obtained in some recently proposed 2D models. They show strong disagreement with the dispersion curve obtained using a simple one-band 2D theory, as well as some discrepancies with respect to the commonly used Das Sarma *et al.*'s dispersion curve, even in the isotropic region. Excellent agreement of the calculated spectrum in pristine graphene with the electron energy loss spectroscopy spectrum measured for lower momentum transfers is demonstrated.

DOI: 10.1103/PhysRevB.87.075447 PACS number(s): 73.22.Pr, 73.22.Lp

I. INTRODUCTION

Since its discovery by Novoselov[1–4] in 2005, graphene has become a very interesting material that is applicable in various fields. As it becomes easier to produce,[1,5,6] this trend is increasing, making graphene applicable in the fields such as photonics,[7] plasmonics,[8,9] or nanoelectronics.[10] Such applications require accurate experimental and theoretical investigations of single particle and collective electronic excitations in graphene, but also their interaction with crystal lattice vibrations, light,[8] etc. Even though there have been many experimental[11–16] and theoretical[14,17–21] studies of various electronic excitations in graphene, there is still a need for accurate first principles calculations of these excitations and their mutual interplay.

In this paper the dynamical response function of graphene is calculated in the first principles density functional theory (DFT), within the random phase approximation (RPA). Using this response function we calculate the propagator of the dynamically screened Coulomb interaction, and then use its imaginary part to obtain the spectra of electronic excitations in graphene. By scanning the intensities of the energy dissipation peaks for each (Q,ω) electronic mode, we obtain a map of electron-hole and plasmon excitations in pristine and doped graphene. The dominant modes in pristine graphene are low-energy π and high-energy $\pi+\sigma$ plasmons. For higher momentum transfers in the ΓM direction we found splitting of the π plasmon to the principal π_1 and the low intensity π_2 modes. This effect has already been observed experimentally[21] and explained theoretically.[16] We found that the high-energy $\pi+\sigma$ plasmon strongly decays into a corresponding interband electron-hole continuum and is only well defined in the optical $Q\approx 0$ limit. Our calculation of the π plasmon energy for small momentum transfers gives 4.85 eV, which is in good agreement with the reported experimental values of 4.7 eV (Ref. 14) or 5.1 eV.[15] For the energy of the $\pi+\sigma$ plasmon we get 14.5 eV, which is also in good agreement with the reported experimental values of 14.6 eV (Ref. 14) or 14.5 eV.[15] We also compare the calculated spectrum with the electron energy loss spectroscopy (EELS) spectrum[14] and find the agreement to be excellent. This confirmed the high precision of our calculations, so we extended our study to the doping induced excitations at shorter wavelengths and found two-dimensional (2D) plasmon dispersion anisotropy.

Most of the results concern electronic excitations in the doped graphene. Doping can be achieved in various ways[22] and for different reasons, many of them related to the applications in electronics, e.g., by opening the gap at the Dirac point. Sometimes doping arises from the charge transfer from the substrate,[23] or is combined with the electrostatic field tuning,[24] where electrons are electrostatically injected into a graphene layer on the field-effect transistor (FET) principle. In this latter case the bands near the Dirac point do not change but the Fermi energy moves to the conduction band. We shall therefore assume that the doping corresponds to the change in the (negative) charge carrier density and the Fermi energy. In doped graphene the dominant mode is the low-energy cone or 2D plasmon. Our detailed *ab initio* calculations enabled us to obtain a very accurate 2D plasmon dispersion curve, and to determine the anisotropy of the 2D plasmon, with the dispersion curve in the ΓM direction following the upper intraband edge, while in the ΓK direction it is shifted toward higher energies. This trend has also been experimentally observed.[11,12] We show that the dispersion curve obtained in the simple one-band 2D electron gas theory lies above the *ab initio* dispersion curve in the long wavelength limit. Even for more accurate model theoretical calculations,[17–19] the agreement with our results is only qualitative.

In Sec. II we describe the first principles (DFT) method used to calculate Kohn-Sham (KS) orbitals in graphene, and describe how to use these orbitals to calculate the RPA z-dependent response function, dielectric function, and propagator of the dynamically screened Coulomb interaction. In Sec. III we use the imaginary part of the induced dynamically screened Coulomb interaction to calculate the spectra of

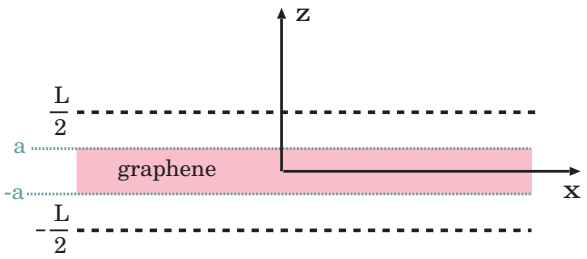

FIG. 1. (Color online) Schematic representation of the graphene monolayer. The unit cell parameter in the parallel direction is $a = 4.651$ a.u., in the perpendicular direction it is $L = 5a$, and the thickness of the electronic density is taken to be $2a$.

electronic excitations in pristine and doped graphene and discuss the obtained spectra. In Sec. IV we present the conclusions.

II. THEORY AND COMPUTATIONAL METHODS

A. Ground state calculation

In this section we briefly describe the calculation of the Kohn-Sham (KS) wave functions and energy levels (band structure) in a graphene monolayer, which are needed to calculate the independent electron response function. A schematic representation of a graphene monolayer is shown in Fig. 1.

For electronic structure calculations we used a plane-wave self-consistent field DFT code (PWSCF), within the Quantum Espresso (QE) package,[25] and the Perdew-Zunger local density approximation (LDA) for the exchange correlation (xc) potential.[26] An electronic temperature of $k_BT \approx 0.1$ eV was assumed to be sufficient to achieve convergence in the calculation of the KS wave functions, and all energies were then extrapolated to 0 K. The ground state electronic density was calculated using a $12 \times 12 \times 1$ Monkhorst-Pack special K-point mesh, i.e., by using 19 special points in the irreducible Brillouin zone shown by the blue squares in Fig. 2.

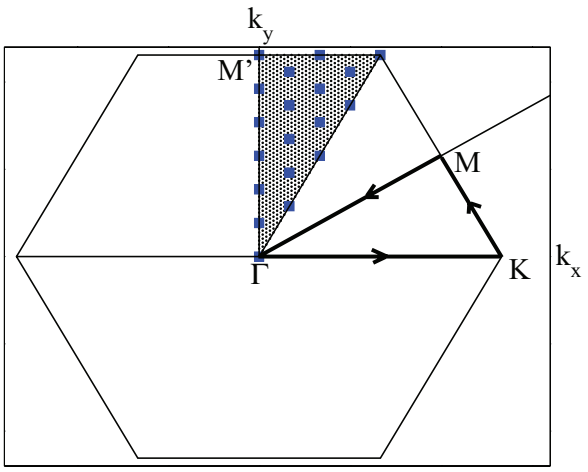

FIG. 2. (Color online) Graphene Brillouin and irreducible Brillouin zone. Blue squares: $12 \times 12 \times 1$ Monkhorst-Pack sampling used in the LDA ground state calculations; black dots: $101 \times 101 \times 1$ Monkhorst-Pack sampling used in the RPA calculation. The thick lines represent the path corresponding to momentum transfers Q for which the loss intensities are calculated and shown in Figs. 5 and 8.

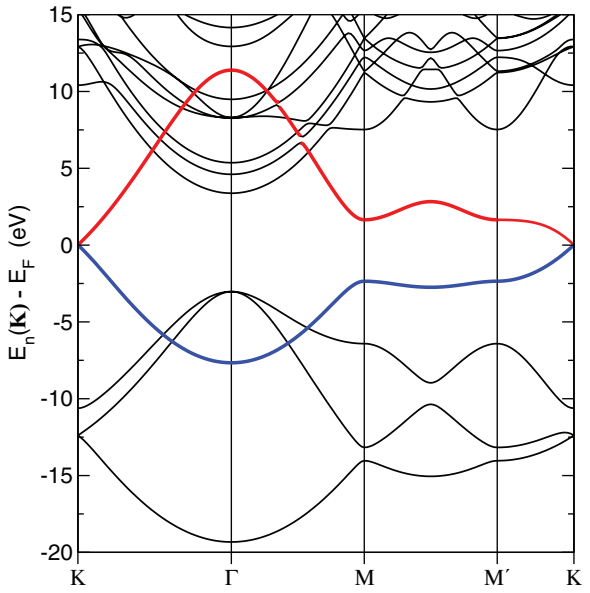

FIG. 3. (Color online) Graphene band structure. The blue line shows the occupied π band and the red line shows the unoccupied π^* band.

In the PWSCF code we used norm-conserving LDA based pseudopotentials for carbon atoms,[27] and we found the energy spectrum to be convergent with a 50 Ry plane-wave cutoff. The graphene band structure along the high symmetry $K\Gamma$, ΓM, MM', and $M'\Gamma$ directions shown in Fig. 3 was calculated along the path with 241 k points, and it agrees with previous calculations.[28] For the graphene unit cell parameter we used $a = 4.651$ a.u., which is the experimental lattice constant commonly used in the literature.[29] For the unit cell in the z direction (separation between periodically repeated graphene layers) we take $L = 5a = 23.255$ a.u., as shown in Figs. 1 and 4. For the response function calculation (as will be explain in Sec. II B) it is important to estimate the appropriate value for the electron density thickness, and we found it to be around $2a$, as shown in Fig. 4.

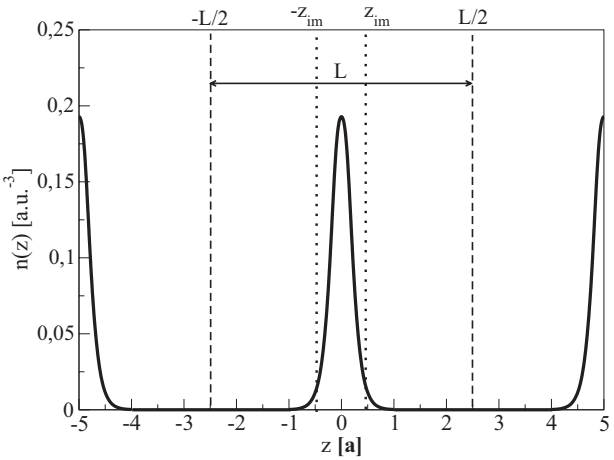

FIG. 4. LDA graphene electronic pseudodensity averaged over the xy plane. L is the thickness of one supercell. The vertical dotted lines represent positions of the image planes in the pristine graphene calculated in Ref. 32. The scale on the abscissa is the unit cell parameter in the xy plane, $a = 4.651$ a.u.

B. Response function calculation

The three-dimensional (3D) Fourier transform of the independent electron response function is given by

$$\chi^0_{\mathbf{GG}'}(\mathbf{Q},\omega) = \frac{2}{V}\sum_{\mathbf{K}\in\mathrm{SBZ}}\sum_{n,m}\frac{f_n(\mathbf{K}) - f_m(\mathbf{K}+\mathbf{Q})}{\omega + i\eta + E_n(\mathbf{K}) - E_m(\mathbf{K}+\mathbf{Q})} \times M_{n\mathbf{K},m\mathbf{K}+\mathbf{Q}}(\mathbf{G})M^*_{n\mathbf{K},m\mathbf{K}+\mathbf{Q}}(\mathbf{G}'), \quad (1)$$

where $V = S * L$ is the normalization volume, S is the normalization surface, and $f_n(\mathbf{K}) = \theta[E_F - E_n(\mathbf{K})]$ is Fermi-Dirac distribution at $T = 0$. In the summation over $\mathbf{K}$ we have used a $101 \times 101 \times 1$ K-point mesh sampling which corresponds to 10 303 Monkhorst-Pack special k points in the Brillouin zone and 901 in the irreducible Brillouin zone shown by the black dots in Fig. 2. Also, the n,m summation is carried out over 20 bands, which proved to be enough for the proper description of the high-energy $\pi + \sigma$ plasmon. The damping parameter η used in this calculation is 100 meV. The matrix elements in (1) have the form

$$M_{n\mathbf{K},m\mathbf{K}+\mathbf{Q}}(\mathbf{G}) = \langle\Phi_{n\mathbf{K}}|e^{-i(\mathbf{Q}+\mathbf{G})\mathbf{r}}|\Phi_{n\mathbf{K}+\mathbf{Q}}\rangle_V, \quad (2)$$

where $\mathbf{Q}$ is the momentum transfer vector parallel to the x-y plane, $\mathbf{G} = (\mathbf{G}_\parallel, G_z)$ are 3D reciprocal lattice vectors, and $\mathbf{r} = (\boldsymbol{\rho}, z)$ is a 3D position vector. Integration is performed over the normalization volume V. The plane-wave expansion of the wave function has the form

$$\Phi_{n\mathbf{K}}(\boldsymbol{\rho},z) = \frac{1}{\sqrt{V}}e^{i\mathbf{K}\boldsymbol{\rho}}\sum_{\mathbf{G}}C_{n\mathbf{K}}(\mathbf{G})e^{i\mathbf{G}\mathbf{r}},$$

where the coefficients $C_{n\mathbf{K}}$ are obtained by solving the LDA-KS equations self-consistently. The above definition of the free response function is standard in supercell approaches where χ_0 is periodically repeated from supercell to supercell (in this case periodically repeated graphene layers), as shown in Fig. 4. The disadvantage of this method is that the calculation of the interacting electron response function χ of an isolated supercell is not straightforward because of the interaction between the supercells. Because of that, it is necessary to minimize or avoid the interaction between the supercells, e.g., by using a truncated bare Coulomb propagator,[30] or by using a "zero padding" method,[31] or simply by using a very large unit cell parameter L in the z direction. On the other hand, the supercell method has an advantage that the calculation can be carried out entirely in the reciprocal space.

In this paper we use an alternative procedure which allows the graphene response function χ to be completely independent of other graphene layers in the superlattice. Also, this method permits the external dynamical charge distribution to be placed anywhere in space, but to excite only the electronic modes inside the corresponding graphene layer, which is very useful in the investigation of various loss mechanisms. The price is that the equations are then more complex, i.e., they are partially in reciprocal and partially in direct space.

The first step in this procedure is the Fourier expansion of the free electron response function (1) in the z,z' directions,

$$\chi^0_{\mathbf{G}_\parallel\mathbf{G}'_\parallel}(\mathbf{Q},\omega,z,z') = \sum_{G_zG'_z}\chi^0_{\mathbf{GG}'}(\mathbf{Q},\omega)e^{iG_zz - iG'_zz'}. \quad (3)$$

The response function (3) is periodic in the z,z' directions and represents the polarizability of noninteracting electrons with the periodically distributed density, such that the densities in different layers do not overlap, as shown in Fig. 4. The z,z' dependence of the total free electron response function can then be written as

$$\chi^0(z,z') = \sum_{n=-\infty}^{\infty}\chi^0_L(z - nL, z' - nL), \quad (4)$$

where $\chi^0_L(z,z')$ represents the response function of noninteracting electrons restricted to the interval $-L/2 < z,z' < L/2$. As a consequence of this, the induced potential coming from the polarization of electrons placed in the interval $-L/2 < z,z' < L/2$ produced by a test charge placed at z can be calculated by using the expression

$$W^{\mathrm{ind}}_{\mathbf{G}_\parallel}(\mathbf{Q},\omega,z,z') = \int_{-L/2}^{L/2}dz_1dz_2\, v^{\mathrm{2D}}_{\mathbf{G}_\parallel}(\mathbf{Q},z,z_1)\chi^0_{\mathbf{G}_\parallel 0} \times (\mathbf{Q},\omega,z_1,z_2)v^{\mathrm{2D}}_0(\mathbf{Q},z_2,z'), \quad (5)$$

where $v^{\mathrm{2D}}_{\mathbf{G}_\parallel}(\mathbf{Q},z,z') = \frac{2\pi}{|\mathbf{Q}+\mathbf{G}_\parallel|}e^{-Q|z-z'|}$ is a 2D Fourier transform of the bare Coulomb interaction. It should be noted here that the general property of a linear superposition of independent response functions (4) is that the integration from $-L/2$ to $L/2$ excludes contributions from the polarization of other layers. This property is very useful in the next step, which is the construction of the interacting electron response function. In order to take into account the electron-electron interaction in (5) we replace the free electron response function $\chi^0_{\mathbf{G}_\parallel\mathbf{G}'_\parallel}$ with the RPA response function $\chi_{\mathbf{G}_\parallel\mathbf{G}'_\parallel}$ obtained as the solution of the Dyson equation

$$\chi_{\mathbf{G}_\parallel\mathbf{G}'_\parallel}(\mathbf{Q},\omega,z,z') = \chi^0_{\mathbf{G}_\parallel\mathbf{G}'_\parallel}(\mathbf{Q},\omega,z,z') + \sum_{\mathbf{G}_{\parallel 1}}\int_{-L/2}^{L/2}dz_1dz_2 \times \chi^0_{\mathbf{G}_\parallel\mathbf{G}_{\parallel 1}}(\mathbf{Q},\omega,z,z_1)v^{\mathrm{2D}}_{\mathbf{G}_{\parallel 1}} \times (\mathbf{Q},z_1,z_2)\chi_{\mathbf{G}_{\parallel 1},\mathbf{G}'_\parallel}(\mathbf{Q},\omega,z_2,z'). \quad (6)$$

Since the integrations in (6) are performed from $-L/2$ to $L/2$, the interaction of the density fluctuations created in the corresponding graphene layer (completely independent of other layers) via the Coulomb propagator $v^{\mathrm{2D}}_{\mathbf{G}_{\parallel 1}}(\mathbf{Q},z_1,z_2)$ is only possible with the density fluctuations within the same layer, and the interaction with the polarization in surrounding layers is completely excluded. This means that from this point on, our calculation is actually performed for a single graphene layer, and it does not depend on the choice of L, assuming that L is large enough to avoid the overlap of the electron orbitals in adjacent layers.

Using the Fourier expansion (3), and a similar one for χ, the Dyson equation (6) becomes a matrix equation,

$$\chi_{\mathbf{G}\mathbf{G}'}(\mathbf{Q},\omega) = \chi^0_{\mathbf{G}\mathbf{G}'}(\mathbf{Q},\omega) + \sum_{\mathbf{G}_1\mathbf{G}_2} \chi^0_{\mathbf{G}\mathbf{G}_1}(\mathbf{Q},\omega) V_{\mathbf{G}_1\mathbf{G}_2} \times (\mathbf{Q}) \chi_{\mathbf{G}_2\mathbf{G}'}(\mathbf{Q},\omega), \quad (7)$$

where the Coulomb interaction matrix elements have the explicit form

$$V_{\mathbf{G}_1\mathbf{G}_2}(\mathbf{Q}) = \frac{4\pi}{|\mathbf{Q}+\mathbf{G}_1|^2}\delta_{\mathbf{G}_1\mathbf{G}_2} - p_{G_{z1}} p_{G_{z2}} \frac{4\pi(1-e^{-|\mathbf{Q}+\mathbf{G}_{\parallel 1}|L})}{|\mathbf{Q}+\mathbf{G}_{\parallel 1}|L} \times \frac{|\mathbf{Q}+\mathbf{G}_{\parallel 1}|^2 - G_{z1}G_{z2}}{\left(|\mathbf{Q}+\mathbf{G}_{\parallel 1}|^2 + G^2_{z1}\right)\left(|\mathbf{Q}+\mathbf{G}_{\parallel 1}|^2 + G^2_{z2}\right)}\delta_{\mathbf{G}_{\parallel 1}\mathbf{G}_{\parallel 2}}, \quad (8)$$

with

$$p_{G_z} = \begin{cases} 1, & G_z = \frac{2k\pi}{L}, \\ -1, & G_z = \frac{(2k+1)\pi}{L}, \end{cases} \quad k = 0,1,2,3,\ldots.$$

The solution of Eq. (7) has the form

$$\chi_{\mathbf{G}\mathbf{G}'}(\mathbf{Q},\omega) = \sum_{\mathbf{G}_1} \mathcal{E}^{-1}_{\mathbf{G}\mathbf{G}_1}(\mathbf{Q},\omega)\chi^0_{\mathbf{G}_1\mathbf{G}'}(\mathbf{Q},\omega), \quad (9)$$

where we have introduced the dielectric matrix

$$\mathcal{E}_{\mathbf{G}\mathbf{G}'}(\mathbf{Q},\omega) = \delta_{\mathbf{G}\mathbf{G}'} - \sum_{\mathbf{G}_1} V_{\mathbf{G}\mathbf{G}_1}(\mathbf{Q})\chi^0_{\mathbf{G}_1\mathbf{G}'}(\mathbf{Q},\omega). \quad (10)$$

As we have already explained, the supercell parameter L in the response function calculation only needs to ensure that electronic densities do not overlap. In Fig. 4 we see that the distance from the graphene center at which the electronic density practically vanishes is comparable to one parallel unit cell a, i.e., $z \approx 5$ a.u. However, we also have to consider the range of induced densities constructed from the unoccupied states which spread through the whole superlattice. Based on previous experience we estimate that the induced density spreads are slightly thicker, or even of the same size, as the ground state density. For example, in Ref. 32 we found that the effective graphene image plane (which represents the centroid of the charge induced by an external point charge) is placed at about 2 a.u. from the graphene center, as denoted in Fig. 4. Finally, to ensure that the graphene RPA response function is completely independent of other layers, we have taken the unit cell thickness to be $L = 23.255$ a.u., which corresponds to five unit cell parameters in the parallel direction, as shown in Fig. 4. We have neglected the local crystal field effects in the parallel but not in the perpendicular direction. This approximation is valid only for small values of Q, but this is exactly the region where we study the interesting features in the low-energy 2D plasmon. We have used the energy of 20 hartrees as the cutoff for the Fourier expansion over G_z's, which corresponds to 47 G_z vectors. This cutoff proved to be sufficient to give a smooth, monotonically decaying asymptotic behavior of the induced charge density for $z > a$.

C. Spectral function calculation

The propagator of the induced dynamically screened Coulomb interaction has the form[33]

$$W^{\text{ind}}_{\mathbf{G}_\parallel}(\mathbf{Q},\omega,z,z') = \int_{-L/2}^{L/2} dz_1 dz_2\, v^{\text{2D}}_{\mathbf{G}_\parallel}(\mathbf{Q},z,z_1)\chi_{\mathbf{G}_\parallel 0} \times (\mathbf{Q},\omega,z_1,z_2) v^{\text{2D}}_0(\mathbf{Q},z_2,z'), \quad (11)$$

where

$$v^{\text{2D}}_{\mathbf{G}_\parallel}(z,z') = \frac{2\pi}{|\mathbf{Q}+\mathbf{G}_\parallel|} e^{-|\mathbf{Q}+\mathbf{G}_\parallel||z-z'|} \quad (12)$$

and index zero means that $\mathbf{G}'_\parallel = 0$. After using expansion (3) [where the independent electron response matrix χ^0 should be replaced by the RPA response matrix (9)] and (12), the integrations over z_1 and z_2 can be performed analytically. Then the induced dynamically screened interaction at $z = z' = 0$ (i.e., in the middle of the graphene monolayer) can be written as

$$W^{\text{ind}}_{\mathbf{G}_\parallel}(\mathbf{Q},\omega,z=0,z'=0) = \sum_{G_{z1}G_{z2}} \chi_{\mathbf{G}_\parallel,0,G_{z1},G_{z2}}(\mathbf{Q},\omega) F_{G_{z1}}(\mathbf{Q}+\mathbf{G}_\parallel) F_{G_{z2}}(\mathbf{Q}), \quad (13)$$

where the form factors F are

$$F_{G_z}(\mathbf{Q}) = \frac{4\pi}{\sqrt{L}} \frac{1 - p_{G_z} e^{-\frac{QL}{2}}}{Q^2 + G_z^2}. \quad (14)$$

Again, the subscript zero in matrix χ means that the $\mathbf{G}'_\parallel$ wave vector is equal to zero. The energy dissipation rate of an external perturbation, e.g., described as the $(\mathbf{Q},\omega)$ Fourier component of a flashing point charge [i.e., static point particle with charge oscillating as $\rho(\mathbf{r},t) = \delta(\mathbf{r}-\mathbf{r}_0)\cos(\omega t)$] placed at $z = 0$,[34] is proportional to the imaginary part of the propagator (13). Generally, the $\mathbf{Q}$ Fourier component of the external perturbation can excite electronic modes with wave vectors $\mathbf{Q}+\mathbf{G}$, where $\mathbf{G}$ can be any reciprocal lattice vector. This means that each $\mathbf{Q}$ component simultaneously loses energy to the sum of all $\mathbf{Q}+\mathbf{G}$ modes. However, the energy transfer is most intense to the excitation of the $\mathbf{Q}+\mathbf{G}$ mode with $\mathbf{G}_\parallel = 0$. This means that the spectral function, which defines for which $(\mathbf{Q},\omega)$ the external perturbation loses energy to electronic excitations, can be written as

$$S(\mathbf{Q},\omega) = -\frac{1}{\pi}\text{Im}\, D(\mathbf{Q},\omega), \quad (15)$$

where we introduced the graphene electronic excitation propagator

$$D(\mathbf{Q},\omega) = v_Q^{-1} W^{\text{ind}}_{\mathbf{G}_\parallel=0}(\mathbf{Q},\omega,z=0,z'=0), \quad (16)$$

and where $v_Q = \frac{2\pi}{Q}$. In the next section we shall use (15) and (16) to calculate the intensities of the electronic excitations in pristine and doped graphene.

III. RESULTS

A. Excitation spectra in pristine graphene

In this section we will present the frequency and wave vector dependence of the intensities of electronic excitations in pristine graphene. Since the intensities and frequencies of the

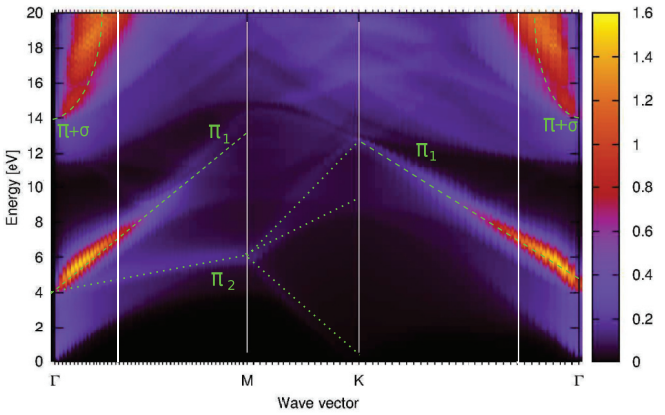

FIG. 5. (Color online) Intensities of the electronic excitations in pristine graphene.

electronic modes depend on the direction of their propagation, the spectra will be investigated along the high symmetry directions ΓM, MK, and $K\Gamma$.

Figure 5 shows the spectrum and intensities of electronic excitations in pristine graphene. The lighter areas indicate the frequencies and wave vectors of the most intense electronic excitations. At lower frequencies in both directions ΓM and $K\Gamma$ we see wide interband $\pi \rightarrow \pi^*$ electron-hole continua forming linearly, increasing the band about 4 eV wide. On the upper edge of this electron-hole continuum we see a π plasmon with very regular linear dispersion, starting from about 4 eV at the Γ point. We notice weak but still noticeable anisotropy of the π plasmon. Namely, in the ΓM direction and for higher wave vectors, starting from $Q \approx 0.2$ a.u., the π plasmon splits, which is not the case in the ΓK direction. In accordance with this, we introduce the notation π_1 for the high-energy dispersed π plasmon, and π_2 for the low-energy, less dispersed plasmon, as indicated in Fig. 5. In Figs. 6(a) and 6(b) we plot the spectra of electronic excitations for particular wave vectors in the ΓM and ΓK directions, respectively, i.e., the intensities of the electronic excitations along the vertical thin dotted lines marked in Fig. 5. We can see that the π_2 plasmon, even though it is weak, influences the intensity and energy of the π_1 plasmon. Namely, for higher wave vectors, the appearance of the π_2 plasmon reduces the intensity of the π_1 plasmon and pushes its dispersion curve toward higher frequencies.

TABLE I. Fitting parameters for various plasmon dispersion curves in pristine graphene in two high symmetry directions ΓM and ΓK.

	Plasmon type					
	π_1		π_2		$\pi + \sigma$	
	ω_π (eV)	v (eV a_0)	ω_π (eV)	v_π (eV a_0)	ω_σ (eV)	v_σ (eV a_0^2)
ΓM	4.3	11.4	4.4	2.6	14.0	270
ΓK	4.3	10.1			14.0	267

We discovered that our numerically calculated plasmon dispersion curves can be very well represented by analytic functions with adjusted parameters, and these fitted curves could be used equally well in the discussion of the results. The dispersion curves of π_1 and π_2 plasmons obtained by tracking the corresponding maxima, shown in Fig. 6, are therefore fitted to the linear curve

$$\omega(Q) = \omega_\pi + v_\pi Q, \tag{17}$$

where ω_π represents the plasmon energy extrapolated to $Q = 0$ and the plasmon group velocity v_π appears as the linear slope of the π plasmon dispersion curve. The π_1 plasmon in the ΓK direction is fitted to just one parameter because the ω_π parameter is set to be equal to the one for the ΓM direction. The fitting parameters for the dispersion curves in both the ΓK and ΓM directions are listed in Table I. There we can see that the slope of the π_1 plasmon in the ΓK direction is slightly reduced compared to the one in the ΓM direction. Also, the slope of the π_2 plasmon is five times smaller than the slope of the π_1 plasmon, i.e., the π_2 plasmon is almost dispersionless, which has been observed experimentally.[16,21] In Table I we also see that the frequency of the π plasmon extrapolated to $Q = 0$ would be $\omega_\pi = 4.3$ eV. This disagreement with the reported experimental values of 4.7 eV (Ref. 14) and 5.1 eV (Ref. 15) arises because for the zero momentum transfer ($Q = 0$) there is no EELS signal and the experimental values of the plasmon frequencies are always measured for some final Q. For example, the resonance at 4.7 eV in Ref. 14 is measured for

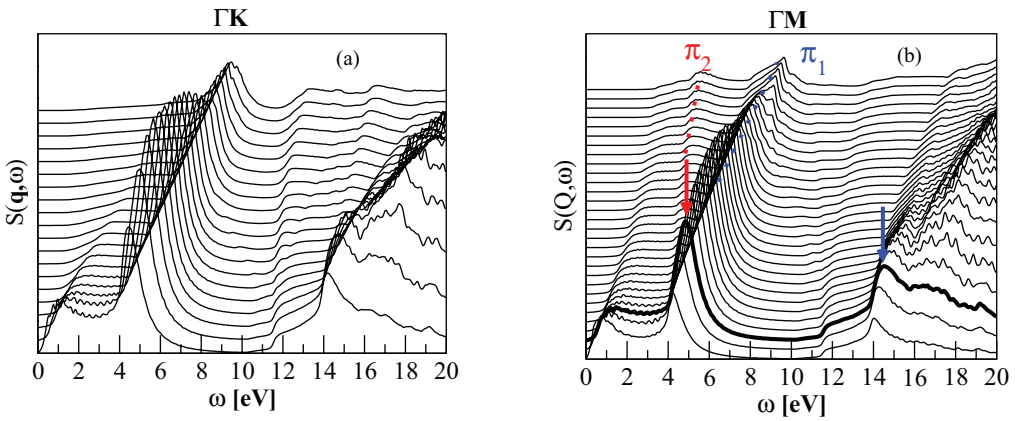

FIG. 6. (Color online) Spectra of electronic excitations in pristine graphene for particular wave vectors $\mathbf{Q}$ in the (a) ΓK and (b) ΓM directions. The minimum absolute value of the wave vectors $\mathbf{Q}$ are for (a) $\Delta Q_{\Gamma M} = 0.0154$ a.u. and for (b) $\Delta Q_{\Gamma K} = 0.02675$ a.u.. For each higher graph the wave vector increases with the corresponding step ΔQ.

the momentum transfer $Q = 0.053$ a.u. in the ΓM direction. The energy of the π_1 plasmon calculated for the closest $Q = 0.046$ a.u., which corresponds to the peak marked with the red arrow in Fig. 6(b), is 4.85 eV, which agrees very well with the experimental value. By using the fitting parameters ω_π and v_π we can also calculate the frequency of the π_1 plasmon exactly at $Q_{\Gamma M} = 0.053$ a.u., which is 4.9 eV.

In Fig. 5, at higher frequencies, starting from about 12 eV at the Γ point, we can see the $\pi \rightarrow \sigma$ electron-hole continuum, increasing more or less quadratically in both the ΓK and ΓM directions. The strong intensity at about 14 eV around the Γ point corresponds to the $\pi + \sigma$ plasmon. In Fig. 6 it can be seen clearly that the $\pi + \sigma$ plasmon is well defined (the high-energy peak) only for very small wave vectors, since very soon it immerses into the $\pi \rightarrow \sigma$ interband electron-hole continuum and decays. Therefore, the dispersion curve of the $\pi + \sigma$ plasmon is fitted to the quadratic curve

$$\omega(Q) = \omega_\sigma + v_\sigma Q^2, \tag{18}$$

but only in the long wavelength ($Q < 0.07$ a.u.) limit, i.e., in the region where the $\pi + \sigma$ plasmon is still well defined. The fitting parameters for the $\pi + \sigma$ plasmon dispersion curves in both the ΓK and ΓM directions are listed in Table I.

ω_σ is the energy of the $\pi + \sigma$ plasmon extrapolated to $Q = 0$, and v_σ represents the quadratic slope of the $\pi + \sigma$ plasmon dispersion curve. The dispersion curve of the $\pi + \sigma$ plasmon in the ΓK direction is fitted to just one parameter because its ω_σ parameter is set to be the same as in the ΓM direction (14 eV). The measured energy of the $\pi + \sigma$ plasmon for momentum transfer $Q = 0.053$ a.u. in the ΓM direction is 14.6 eV,[14] while the value we get for momentum transfer $Q = 0.046$ a.u. [corresponding to the peak marked with a blue arrow in Fig. 6(b)] is 14.5 eV, which is in excellent agreement. Using the fitting parameters ω_σ and v_σ we can also calculate the frequency of the $\pi + \sigma$ plasmon exactly at $Q_{\Gamma M} = 0.053$ a.u., which is 14.8 eV. The quadratic slopes v_σ for both high symmetry directions are very similar, as could be expected, since plasmon dispersion is supposed to be isotropic for small momentum transfers.

To compare the complete calculated spectra directly with experimental ones, it is more convenient to use standard (spatial average) loss theory than this spatially dependent loss formulation. Namely, in EELS experiments the moving electron either passes through or is reflected from graphene, and its losses do not correspond to the losses of a flashing point charge placed at $z = 0$ (what we calculate here). Therefore, to be more consistent with the experiment, instead of putting $z = 0$ and $z' = 0$ [as in (16)] it is better to calculate the average values over z and z'. In that case the loss function can be written in terms of inverted dielectric matrix (10),

$$S(Q,\omega) = -\mathrm{Im}\, \mathcal{E}^{-1}_{\mathbf{G}=0\mathbf{G}'=0}(\mathbf{Q},\omega). \tag{19}$$

The detailed derivation of the loss function (19) from the spatially dependent loss function (15) is presented in Ref. 31. A comparison between the experimental[14] and the theoretical spectrum obtained from expression (19) is shown in Fig. 7. In the calculation of χ_0 we have increased the damping parameter η to 500 meV to take account of the experimentally observed broadening.

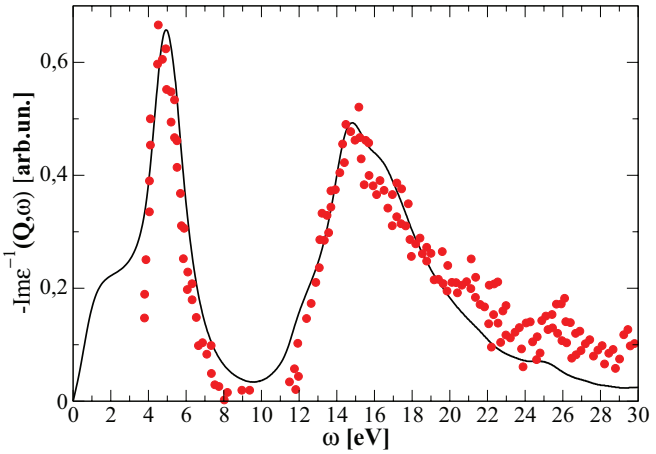

FIG. 7. (Color online) Comparison between the spectrum of electronic excitations in pristine graphene calculated from (19) for $\mathbf{Q} = 0.046$ a.u. in the ΓM direction and the experimental results taken from Ref. 14, where $\mathbf{Q} = 0.053$ a.u., also in the ΓM direction.

As can be noticed, the experimental spectrum agrees very well with the spectrum obtained from expression (19). Using a larger number of bands, the high-energy tail of the $\pi + \sigma$ plasmon would slightly increase, causing a small redshift of the π plasmon peak due to the conservation of the spectral weight. This would lead to an even better agreement with the experimental spectrum, but that is not the topic of this paper.

In Fig. 5 we can also notice some weak but interesting (since they appear at large Q) spectral intensities between the M and K points, which we have marked by thin dotted lines. We do not know the exact origin of these structures, but we assume that they originate from various interband transitions with very low intensity due to the large momentum transfers.

B. Excitation spectra in doped graphene

We can use expression (15) to calculate the spectrum of electronic excitations in doped graphene as well. The intensities of the electronic excitations for the doping parameter $E_F = 1$ eV are shown in Fig. 8. Since doping does not affect the high-energy part of the spectrum, the intensities of the electronic modes are plotted only up to 10 eV. Also, since there

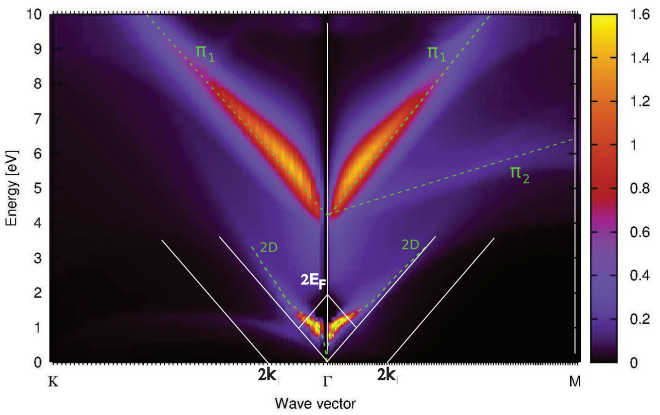

FIG. 8. (Color online) Intensities of electronic excitations in doped graphene, $E_F = 1$ eV.

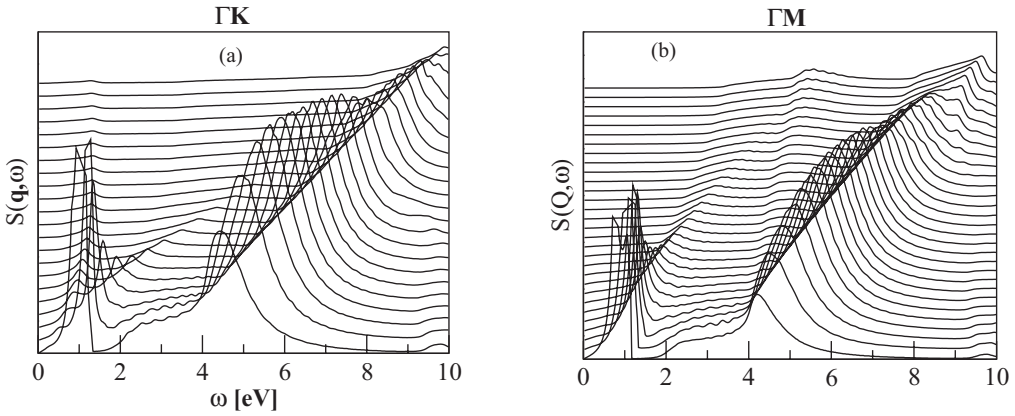

FIG. 9. Spectra of electronic excitations in doped graphene ($E_F = 1$ eV) for particular wave vectors $\mathbf{Q}$ in the (a) ΓK and (b) ΓM directions. The corresponding absolute values of the wave vectors are the same as in Fig. 6.

are no interesting doping induced structures in the low-energy region for momentum transfers in the KM direction, the spectra are presented only in the ΓK and ΓM directions.

We can again clearly see the intense π_1 and weak π_2 plasmons, but our attention will now focus on the low-energy part of the spectrum. First of all, we see that the region of $\pi \to \pi^*$ interband electron-hole transitions is shifted to higher energies. Its lower edge starts from $\omega = 2E_F$ at the Γ point and the slope is negative. Since now the π^* band is partially filled, there is also a $\pi^* \to \pi^*$ intraband electron-hole continuum with the upper edge starting from $\omega = 0$ at the Γ point and positive dispersion. At $\omega = E_F$ the upper edge of the $\pi^* \to \pi^*$ electron-hole continuum joins with the lower edge of the $\pi \to \pi^*$ electron-hole continuum, and in the region between there is a gap which can be seen for small energies and momentum transfers as the black region in Fig. 8. Within this gap there is a very strong (very light line starting from $Q = 0$) 2D plasmon. Also, we can see that the 2D plasmon is strong only for very low wave vectors, while at about $Q = 0.1$ a.u. it merges with the lower edge of the $\pi \to \pi^*$ electron-hole continuum, which reduces its intensity substantially.

This 2D plasmon is the main difference between collective excitations in pristine and doped graphene. It appears due to the intraband transitions, and in the long wavelength limit it follows the $\sqrt{2E_F Q}$ dispersion, analogous to the one in a 2D free electron gas. With increasing Q this plasmon is modified with respect to the 2D free electron gas, because the electron dispersion (Dirac cone) near the Fermi energy is different, and gradually it also involves contributions from the interband transitions (transitions between the lower and upper cones). Also, it should be emphasized that in pristine graphene the lowest-energy plasmon is a π plasmon, starting at around 5 eV.

In Fig. 9 we present the spectra of electronic excitations for particular wave vectors in the ΓK and ΓM directions. Here we can see more clearly how the intensity of the 2D plasmon suddenly decreases at about $Q \approx 0.1$ a.u. [corresponding to the fourth spectrum in Fig. 9(a) or the seventh spectrum in Fig. 9(b)]. For the higher-energy range, $\omega \gtrsim 4$ eV, in Fig. 9 we can see peaks corresponding to the π_1 plasmon with the dispersion curve linear in the ΓK direction, and its deviation with respect to the linear behavior in the ΓM direction is attributed to the influence of the weak π_2 plasmon.

In Fig. 8 we can see noticeable anisotropy of the low-energy part of the spectrum. First of all, the upper edge of the $\pi^* \to \pi^*$ intraband electron-hole continuum has a higher slope in the ΓK than in the ΓM direction. This is probably due to the anisotropy of π and π^* bands around the K point, and it has consequences for the 2D plasmon which, for higher momentum transfers, follows the upper edge of the $\pi^* \to \pi^*$ electron-hole continuum,[17] and therefore also becomes anisotropic. Furthermore, in Fig. 8 we can also notice an area of low-intensity excitations in the ΓK direction (slightly below the 2D plasmon) with roughly square root dispersion, which does not appear in the ΓM direction.

Figure 10 shows dispersion curves of 2D plasmons obtained by tracking the low-energy maxima in Figs. 8 or 9. The red

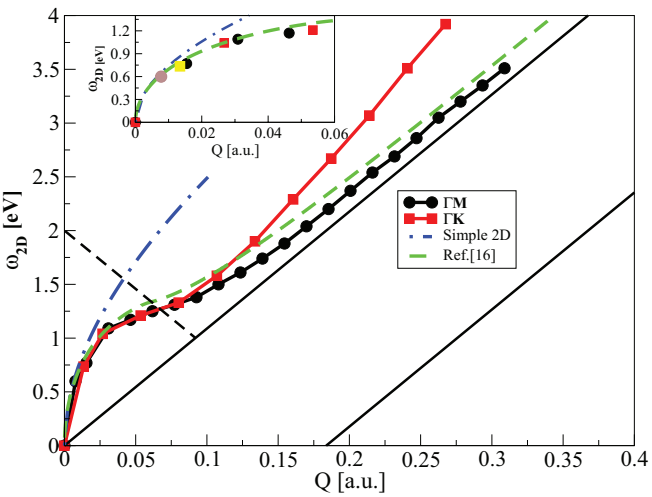

FIG. 10. (Color online) Dispersion curve of a 2D plasmon in doped graphene. Red squares: Frequencies of the low-energy peaks in Fig. 9(a); black dots: frequencies of the low-energy peaks in Fig. 9(b); blue dotted-dashed line: one-band model dispersion curve (27); green dashed line: dispersion curve obtained by using a free electron response function taken from Ref. 17. The solid lines denote the borders of the intraband electron-hole region and the dashed line with a negative slope represents the lower interband electron-hole edge. The inset shows the frequencies of 2D plasmons calculated for very low momentum transfers, $Q_{\Gamma M} = 0.0078$ a.u. (brown dot) and $Q_{\Gamma K} = 0.0134$ a.u. (yellow square).

squares represent the frequencies of the low-energy peaks in Fig. 9(a) and the black dots represent the frequencies of the low-energy peaks in Fig. 9(b). The region between thick solid lines is the $\pi^* \to \pi^*$ intraband electron-hole continuum and the thick dashed line represents the lower edge of the $\pi \to \pi^*$ interband electron-hole continuum with negative dispersion, as described above. We see that the dispersion curve is isotropic (the dispersion curves in the ΓK and ΓM directions overlap exactly), with a square root behavior until it reaches the lower interband edge. After that the dispersion curves split: The dispersion curve in the ΓM direction continues to follow the upper intraband edge, while the dispersion curve in the ΓK direction moves towards higher frequencies. It is important to notice that this effect also has been experimentally observed and presented in Fig. 2 in Ref. 11 or in Fig. 5 in Ref. 12, where experimental frequencies for wave vectors in the ΓK direction first follow the theoretical curve taken from Ref. 17 and then, as they enter the interband region, suddenly split from the theoretical curve (which approximately follows our dispersion curve in the ΓM direction) and move towards higher frequencies. The anisotropy of the 2D plasmon has already been suggested in Ref. 18, but, in our opinion, it was based on an unconvincing theoretical analysis.

In Fig. 10 we see that the 2D plasmon is isotropic only for very small momentum transfers, $Q < 0.075$ a.u., before entering the intraband transition region, i.e., as long as it is well defined as the collective excitation (as can be seen in Figs. 8 and 9). In other words, for small momentum transfers the 2D plasmon can be treated as an isotropic excitation and our results can be compared with those obtained by simple 2D models.

C. Comparison with 2D models

As we have already explained, in the long wavelength limit the dispersion of the 2D plasmon is isotropic and we can also call it the "isotropic region." To illustrate this, we will use the 2D model of Ref. 17 in the framework of the tight binding model, so the Hamiltonian describing the electrons in the vicinity of the K and K' points can be written as

$$H_K(\mathbf{K}) = -H_{K'}^T(\mathbf{K}) = \gamma K \begin{bmatrix} 0 & e^{-i\theta_{\mathbf{K}}} \\ e^{i\theta_{\mathbf{K}}} & 0 \end{bmatrix}, \tag{20}$$

where $\mathbf{K} = (K_x, K_y)$ is a two-dimensional wave vector, $\theta_{\mathbf{K}} = \arctan\frac{K_y}{K_x}$ is the mixing parameter of two carbon π orbitals in the primitive cell, $\gamma = \frac{3ta}{2}$, where $t = 2.7$ eV is hopping parameter and a is the unit cell constant. A solution of this Hamiltonian in the continuum approximation ($\mathbf{R} \to \boldsymbol{\rho}$, where $\mathbf{R}$ is the 2D translation vector) is given by

$$E_{\mathbf{K}s} = s\gamma K \tag{21}$$

and

$$|\mathbf{K}s\rangle = \frac{1}{\sqrt{2S}} e^{i\mathbf{K}\boldsymbol{\rho}} \begin{pmatrix} 1 \\ s e^{i\theta_{\mathbf{K}}} \end{pmatrix}, \tag{22}$$

where s is the band index: $s = -1$ denotes π while $s = 1$ denotes the π^* band. The column matrix is a combination of pseudospinors $\binom{1}{0}$ and $\binom{0}{1}$ representing two structureless π orbitals in the primitive cell. The independent electron response function which includes electron-hole transitions around the K and K' points can then bewritten as

$$\chi^0(Q,\omega) = \frac{g_s g_v}{S} \sum_{\mathbf{K}ss'} \frac{f_{\mathbf{K}s} - f_{\mathbf{K}+\mathbf{Q}s'}}{\omega + E_{\mathbf{K}s} - E_{\mathbf{K}+\mathbf{Q}s'} + i\eta} \times |F_{ss'}(\mathbf{K},\mathbf{K}+\mathbf{Q})|^2, \tag{23}$$

where $f_{\mathbf{K}} = \theta(E_F - E_{\mathbf{K}})$ is the Fermi-Dirac distribution at $T = 0$, and $g_s = 2$ is the spin and $g_v = 2$ is valley degeneracy, since the contribution of the electrons around the K and K' points is the same. The overlap matrix elements are given by

$$|F_{ss'}(\mathbf{K},\mathbf{K}+\mathbf{Q})|^2 = \tfrac{1}{2}(1 + ss' \cos\theta_{\mathbf{K},\mathbf{K}+\mathbf{Q}}),$$

where $\theta_{\mathbf{K},\mathbf{K}+\mathbf{Q}} = \theta_{\mathbf{K}+\mathbf{Q}} - \theta_{\mathbf{K}}$. The response function (23) includes all possible intra- and interband transitions between the π and π^* bands. For example, the $s = s'$ terms represent intraband transitions where for negative doping ($E_F < 0$) only the $s = s' = -1$ term contributes, while for positive doping ($E_F > 0$) only the $s = s' = 1$ term contributes. Interband $s \neq s'$ terms are always active and they are the only contributing terms in the pristine graphene.

Since we use positive doping, $E_F = 1$ eV, we will first examine if the $\pi^* \to \pi^*$ intraband electron-hole transitions alone are sufficient to reproduce an *ab initio* 2D plasmon dispersion curve in the long wavelength limit. Assuming that the overlap matrix elements $|F_{11}(\mathbf{K},\mathbf{K}')|^2$ are equal to one, and keeping only the $s = s' = 1$ term in the response function (23), it becomes

$$\chi^0(Q,\omega) = \frac{g_s g_v}{S} \sum_{\mathbf{K}} \frac{f_{\mathbf{K}} - f_{\mathbf{K}+\mathbf{Q}}}{\omega + E_{\mathbf{K}} - E_{\mathbf{K}+\mathbf{Q}} + i\eta}. \tag{24}$$

In the long wavelength limit the $\mathbf{K}$ integration can be performed analytically, and keeping the terms up to Q^4 we get[35]

$$\mathrm{Re}\,\chi^0(Q,\omega) \approx \frac{k_F^2}{\pi E_F}\left[\frac{Q^2}{\omega^2} + \frac{3}{4}\frac{Q^4}{\omega^4}\right], \tag{25}$$

where $k_F = \frac{E_F}{\gamma}$. The dispersion relation of the 2D plasmon can now be obtained by solving the equation

$$\epsilon(Q,\omega) = 1 - v_Q\,\mathrm{Re}\,\chi^0(Q,\omega) = 0, \tag{26}$$

which can be done analytically to get

$$\omega(Q) = \sqrt{2E_F Q + \frac{3}{4}\gamma^2 Q^2 - \frac{9}{32}\frac{\gamma^4}{E_F}Q^3}. \tag{27}$$

The plasmon dispersion relation obtained from (27) is presented by the blue dotted-dashed line in Fig. 10. We can see a significant discrepancy with respect to the *ab initio* dispersion curve which suggests that the one-band 2D theory is not sufficient to describe the 2D plasmon in graphene, not even in the region where the 2D plasmon is still not influenced by $\pi \to \pi^*$ interband electron-hole transitions. To show that the discrepancy is noticeable even for very small wave vectors, we increased the K-point mesh sampling in the *ab initio* calculation of χ^0 [Eq. (1)] to $201 \times 201 \times 1$, which enabled us to calculate the energies of the 2D plasmon for very small momentum transfers. In the insert of Fig. 10 the first (brown dot) and second (yellow square) calculated points represent

frequencies of the 2D plasmon for $Q_{\Gamma M} = 0.0078$ a.u. and $Q_{\Gamma K} = 0.0134$ a.u., respectively. We see that the blue dotted-dashed curve (27) passes through the first $Q_{\Gamma M}$ point, but lies above the next, $Q_{\Gamma K} = 0.0134$ a.u., point. Obviously, for a better description of the 2D plasmon dispersion, the contributions of both the π and π^* bands and proper overlap matrix elements between these states should be taken into account.

The dispersion curve obtained by solving (26) and using the complete response function (23), including all allowed intra- and interband transitions, corresponds to the one published in Ref. 17, and is presented by a green dashed line in Fig. 10. We see that this curve passes almost exactly through our points up to $Q \approx 0.04$ a.u., but then goes above the *ab initio* calculations and follows our curve at the same distance for all wave vectors. It is interesting that in the anisotropic region (interband region) it follows the dispersion curve in the ΓM direction, as well as the upper intraband edge. This is consistent with experimental results[11,12] for dispersion in the ΓK direction. The experimental curve first agrees with the 2D theoretical curve taken from Ref. 17 and then, as it enters the anisotropic region, changes direction toward higher frequencies (just as our dispersion curve in the ΓK direction) while the theoretical curve continues to follow the upper intraband edge. We are not aware of any experimental results for dispersion in the ΓM direction so we cannot verify if it follows the upper interband edge, as our results suggest. Also, the theoretical dashed-dotted curve in Fig. 2 in Ref. 11 is slightly above the experimental values in the isotropic region, which is also consistent with the results presented here.

We can conclude that the simple 2D theory agrees with the *ab initio* dispersion curve only in the $Q \approx 0$ region, while the 2D theory taken from Ref. 17 gives better agreement, but still not in the whole isotropic region. Obviously, for a proper description of 2D plasmon dispersion one should take into account more realistic π orbitals and matrix elements between them.

IV. CONCLUSIONS

In this paper we have systematically analyzed the spectra of electronic excitations in pristine and doped graphene. We obtained energies of the π and $\pi + \sigma$ plasmons around the Γ point which agree with experimental values, as well as anisotropy and splitting of the π plasmon which is also experimentally verified. Moreover, the high accuracy of the calculation enabled us to discover some different features in the spectra, e.g., the ΓM-ΓK anisotropy of the 2D plasmon dispersion curve which has been only partially experimentally verified. Also, we compared our *ab initio* 2D plasmon dispersion curves with the dispersion curves obtained by using some recently proposed 2D models, and found not only strong disagreement with the simple one-band 2D theory, but also some discrepancies with respect to the commonly used Das Sarma *et al.*'s 2D dispersion, even in the isotropic region. This suggests that there is a need for high resolution experimental measurements of 2D plasmon dispersion curves in doped graphene to verify our theoretical predictions. This can be very important in several fields, such as photonics or plasmonics, where, e.g., in the processes of the light-plasmon (polariton) conversion and vice versa it is very important to know the exact energies and widths of the 2D plasmons.

ACKNOWLEDGMENTS

Two of the authors (V.D. and M.Š.) are grateful to Donostia International Physics Center (DIPC) and Pedro M. Echenique for hospitality during various stages of this research. We also thank D. J. Mowbray and V. Silkin for useful discussions.

*vito@phy.hr

[1] K. S. Novoselov, A. K. Geim, S. V. Morozov, D. Jiang, M. I. Katsnelson, I. V. Grigorieva, S. V. Dubonos, and A. A. Firsov, Nature (London) **438**, 197 (2005).

[2] Y. Zhang, Y. W. Tan, H. L. Stormer, and P. Kim, Nature (London) **438**, 201 (2005).

[3] K. S. Novoselov, A. K. Geim, S. V. Morozov, D. Jiang, Y. Zhang, S. V. Dubonos, I. V. Grigorieva, and A. A. Firsov, Science **306**, 666 (2004).

[4] K. S. Novoselov, D. Jiang, F. Schedin, T. J. Booth, V. V. Khotkevich, S. V. Morozov, and A. K. Geim, Proc. Natl. Acad. Sci. USA **102**, 10451 (2005).

[5] A. K. Geim and K. S. Novoselov, Nat. Mater. **6**, 183 (2007).

[6] I. Pletikosic, M. Kralj, P. Pervan, R. Brako, J. Coraux, A. T. N'Diaye, C. Busse, and T. Michely, Phys. Rev. Lett. **102**, 056808 (2009).

[7] F. Bonaccorso, Z. Sun, T. Hasan, and A. C. Ferrari, Nat. Photonics **4**, 611 (2010).

[8] M. Jablan, H. Buljan, and M. Soljačić, Phys. Rev. B **80**, 245435 (2009).

[9] F. H. L. Koppens, D. E. Chang, and F. J. Garcia de Abajo, Nano Lett. **11**, 3370 (2011).

[10] Y. Zhang, T. T. Tang, Ç. Ö. Girit, Z. Hao, M. C. Martin, A. Zettl, M. F. Crommie, Y. R. Shen, and F. Wang, Nature **459**, 820 (2009).

[11] C. Tegenkamp, H. Pfnur, T. Langer, J. Baringhaus, and H. W. Schumacher, J. Phys.: Condens. Matter **23**, 012001 (2011).

[12] T. Langer, J. Baringhaus, H. Pfnur, H. W. Schumacher, and C. Tegenkamp, New J. Phys. **12**, 033017 (2010).

[13] Y. Liu, R. F. Willis, K. V. Emtsev, and Th. Seyller, Phys. Rev. B **78**, 201403 (2008); S. Y. Shin, C. G. Hwang, S. J. Sung, N. D. Kim, H. S. Kim, and J. W. Chung, *ibid.* **83**, 161403 (2011).

[14] T. Eberlein, U. Bangert, R. R. Nair, R. Jones, M. Gass, A. L. Bleloch, K. S. Novoselov, A. Geim, and P. R. Briddon, Phys. Rev. B **77**, 233406 (2008).

[15] J. Lu, K. P. Loh, H. Huang, W. Chen, and A. T. S. Wee, Phys. Rev. B **80**, 113410 (2009).

[16] C. Kramberger, F. Roth, R. Schuster, R. Kraus, M. Knupfer, E. Einarsson, S. Maruyama, D. J. Mowbray, A. Rubio, and T. Pichler, Phys. Rev. B **85**, 085424 (2012).

[17] E. H. Hwang and S. Das Sarma, Phys. Rev. B **75**, 205418 (2007); **80**, 205405 (2009).

[18] Y. Gao and Z. Yuan, Solid State Commun. **151**, 1009 (2011).

[19] V. B. Jovanović, I. Radović, D. Borka, and Z. L. Mišković, Phys. Rev. B **84**, 155416 (2011).

[20] M. Polini, R. Asgari, G. Borghi, Y. Barlas, T. Pereg-Barnea, and A. H. MacDonald, Phys. Rev. B **77**, 081411(R) (2008).

[21]C. Kramberger, R. Hambach, C. Giorgetti, M. H. Rummeli, M. Knupfer, J. Fink, B. Buchner, L. Reining, E. Einarsson, S. Maruyama, F. Sottile, K. Hannewald, V. Olevano, A. G. Marinopoulos, and T. Pichler, Phys. Rev. Lett. **100**, 196803 (2008).

[22]B. Guo, L. Fang, B. Zhang, and J. R. Gong, Insciences J. **1**, 80 (2011).

[23]L. Kong, C. Bjelkevig, S. Gaddam, M. Zhou, Y. H. Lee, G. H. Han, H. K. Jeong, N. Wu, Z. Zhang, J. Xiao, P. A. Dowben, and J. A. Kelber, J. Phys. Chem. C **114**, 21618 (2010).

[24]M. Bokdam, P. A. Khomyakov, G. Brocks, Z. Zhong, and P. J. Kelly, Nano Lett. **11**, 4631 (2011).

[25]P. Giannozzi, S. Baroni, N. Bonini, M. Calandra, R. Car, C. Cavazzoni, D. Ceresoli, G. L. Chiarotti, M. Cococcioni, I. Dabo *et al.*, J. Phys.: Condens. Matter **21**, 395502 (2009).

[26]J. P. Perdew and A. Zunger, Phys. Rev. B **23**, 5048 (1981).

[27]N. Troullier and J. L. Martins, Phys. Rev. B **43**, 1993 (1991).

[28]P. E. Trevisanutto, C. Giorgetti, L. Reining, M. Ladisa, and V. Olevano, Phys. Rev. Lett. **101**, 226405 (2008); C. Attaccalite, A. Grüneis, T. Pichler, and A. Rubio, arXiv:0808.0786.

[29]R. Saito, G. Dresselhaus, and M. S. Dresselhaus, *Physical Properties of Carbon Nanotubes* (Imperial College Press, London, 1998); M. S. Dresselhaud, G. Dresselhaus, and P. C. Eklund, *Science of Fullerenes and Carbon Nanotubes* (Academic, San Diego, 1996); M. S. Dresselhaus and G. Dresselhaus, Adv. Phys. **51**, 1 (2002); V. W. Brar, Y. Zhang, Y. Yayon, T. Ohta, J. L. McChesney, A. Bostwick, E. Rotenberg, K. Horn, and M. F. Crommie, Appl. Phys. Lett. **91**, 122102 (2007); S. B. Trickey, F. Müller-Plathe, G. H. F. Diercksen, and J. C. Boettger, Phys. Rev. B **45**, 4460 (1992); J.-C. Charlier, X. Gonze, and J.-P. Michenaud, *ibid.* **43**, 4579 (1991); V. N. Kotov, B. Uchoa, V. M. Pereira, F. Guinea, and A. H. Castro Neto, Rev. Mod. Phys. **84**, 1067 (2012).

[30]C. A. Rozzi, D. Varsano, A. Marini, E. K. U. Gross, and A. Rubio, Phys. Rev. B **73**, 205119 (2006).

[31]D. J. Mowbray, V. Despoja, P. Ayala, T. Pichler, and A. Rubio, *Theoretical Spectroscopy Techniques Applied to Graphene EELS and Optics* (unpublished).

[32]V. Despoja, D. J. Mowbray, D. Vlahović, and L. Marušić, Phys. Rev. B **86**, 195429 (2012).

[33]L. Marušić and M. Šunjić, Phys. Scr. **63**, 336 (2001).

[34]V. Despoja, K. Dekanić, M. Šunjić, and L. Marušić, Phys. Rev. B **86**, 165419 (2012).

[35]K. W.-K. Shung, Phys. Rev. B **34**, 979 (1986).